HIGH-RESOLUTION PHYSICAL AND MAGNETIC PROPERTIES OF RAPIDLY DEPOSITED LAYERS ASSOCIATED WITH LANDSLIDES, EARTHQUAKES AND FLOODS

Guillaume St-Onge
ISMER & GEOTOP, Rimouski, Québec, Canada, guillaume_st-onge@uqar.qc.ca
Emmanuel Chapron
Institut des Sciences de la Terre d'Orléans, UMR 6113 CNRS-Université d'Orléans, France
Hervé Guyard and André Rochon
ISMER & GEOTOP, Rimouski, Québec, Canada
Patrick Lajeunesse
Centre d'études nordiques & Département de géographie, Université Laval, Québec, Québec, Canada
Jacques Locat
Département de géologie & génie géologique, Université Laval, Québec, Québec, Canada
Dave Scott
Centre for Environmental and Marine Geology, Dalhousie University, Halifax, Canada
Joseph S. Stoner
College of Oceanography and Atmospheric Sciences, Oregon State University, Corvallis, Oregon, USA
Claude Hillaire-Marcel
UQAM & GEOTOP, Montréal, Québec, Canada

RÉSUMÉ
Au cours de la dernière décennie, des percées importantes ont été réalisées dans l'analyse en continu des propriétés magnétiques et physiques de carottes sédimentaires. Des analyses rapides et non destructrices peuvent maintenant être réalisées en continu sur des carottes aussi bien marines que lacustres et avec une résolution de l'ordre de 100 µm. Cette très haute résolution spatiale, ainsi que la possibilité d'acquérir des images digitales classiques ou radiographiques de haute résolution, offrent de nouvelles opportunités pour l'identification et la caractérisation de couches sédimentaires associées à des catastrophes naturelles comme les glissements de terrain, séismes et crues. Dans cet article, nous illustrons comment l'analyse des propriétés physiques et magnétiques en continu de carottes sédimentaires peut être utilisée en parallèle avec des analyses sédimentologiques classiques pour identifier et dater des couches accidentelles engendrées par des glissements de terrain, des séismes et des crues. Nous présentons des exemples récents provenant de carottes marines et lacustres de l'est du Canada, de l'Arctique canadien, de la baie et du détroit d'Hudson, de la Patagonie et des Alpes.

ABSTRACT
During the last decade, major technological advances were made regarding the continuous measurement of the physical and magnetic properties of sediment cores. Rapid and non destructive analysis can now be performed continuously on either marine or lacustrine sediments with a downcore resolution of up to 100 µm. Such a resolution in conjunction with the possibility of acquiring high-resolution digital classical or X-ray images of sediment cores allow new opportunities for the identification and characterization of sediment layers associated with natural hazards such as landslides, earthquakes or floods. In this paper, we illustrate how the continuous physical and magnetic properties of the sediments can be combined with classical sedimentological analyses to identify and date rapidly deposited layers triggered by landslides, earthquakes and floods. We provide an overview of several recent examples from marine and lacustrine Holocene sedimentary records from Eastern and Arctic Canada, Hudson Bay and Strait, Patagonia and the Alps.

1. INTRODUCTION

The identification, characterization and dating of sediment layers associated with natural hazards such as landslides, earthquakes or floods are a major step towards establishing the frequency or recurrence of such events. Determining the frequency of natural hazards beyond the historical records is essential to ensure the safety of the public and infrastructures such as dams, bridges, etc.

Major technological advances were recently made regarding the continuous measurement of the physical and magnetic properties of either marine or lacustrine sediment cores with a downcore resolution of up to 100 µm. Such a resolution in conjunction with the possibility of acquiring high resolution digital classical or X-ray images of sediment cores allow to quantify sediment disturbance due to coring and new opportunities in natural hazard research. In this paper, we will present several novel techniques such as CAT-scan (Computerized co-axial tomography), microfluorescence-X, color reflectance and paleomagnetism, and show how they can be combined with classical sedimentological or geochemical analyses to identify and date rapidly deposited layers. We will overview several recent examples previously

In : J. Locat, D. Perret, D. Turmel, D. Demers et S. Leroueil, (2008).
Comptes rendus de la 4e Conférence canadienne sur les géorisques: des causes à la gestion.
Proceedings of the 4th Canadian Conference on Geohazards : From Causes to Management. Presse de l'Université Laval, Québec, 594 p.

published from marine and lacustrine Holocene sedimentary records from Eastern and Arctic Canada, Hudson Bay and Strait, Patagonia and the Alps.

2. MATERIAL AND METHODS

2.1 Core location and sampling

At sea, core 12PC was collected by piston coring in the Gulf of St. Lawrence (Eastern Canada) on board the R/V Coriolis II, whereas cores 124, 750, 27bLEH, 28PC were raised by piston or gravity coring in the Beaufort Sea (124), Amundsen Gulf (750), Hudson Bay (27bLEH) and Strait (28PC) onboard the ice-breaker CCGS Amundsen (Fig. 1 and Table 1). Cores 2222 and 2220 were sampled in the Saguenay Fjord and St. Lawrence Estuary (Quebec, Canada), respectively, using a Calypso piston corer on board the Marion Dufresne II, whereas core 101 was sampled in Hudson Strait very close to core 28PC using a piston core on board the CSS Hudson. In lakes, cores BRA03-1 in Lake Bramant (Massif des Grandes Rousses, French Alps), LDB 11a in Lake Le Bourget (French NW Alps) and PU-I-P4 in Lake Puyehue (Chilean Northern Patagonia) were retrieved using short gravity coring devices either from a platform or from a rubber boat (Fig. 1 and Table 1).

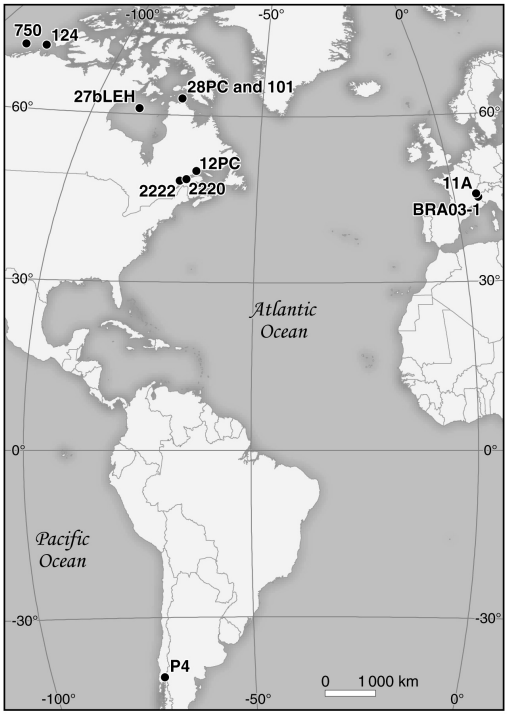

Figure 1. Location of the cores discussed in the text.

Table 1. Name and location of cores discussed in the text.

Core	Name used	Lat./long.	Depth (m)
COR0503-12PC[1]	12PC	50°06'36''N 66°19'43''W	190
AMD0509-28PC[2]	28PC	63°02'49.8''N 74°18'62.9"W	430
AMD0509-27bLEH[2]	27bLEH	61°03'11.8''N 86°12'49.9''W	245
HU90-023-101[3]	101	63°02.99'N 74°18.24'W	389
2004-804-124[4]	124	71°24.8'N 126°46.1'W	426
2004-804-750[4]	750	71°20.45'N 134°06.20'W	1087
BRA03-1[5]	BRA03-1	45°10'20''N 6°10''15''E	36
LDB11a[6]	LDB11a	45°45'30''N 5°51'30''E	146
PU-I-P4[7]	PU-I-P4	40°39''8''S 72°21'10''W	122
MD99-2222[8]	2222	48°18.28'N 70°15.44'W	271
MD99-2220[9]	2220	48°38.32'N 68°37.93'W	320

[1] Lajeunesse *et al.* (2007) [2] St-Onge and Lajeunesse (2007); [3] Kerwin (1996); [4] Scott *et al.* (subm.); [5] Guyard *et al.* (2007a); [6] Chapron *et al.* (1999); [7] Chapron *et al.* (2007); [8] St-Onge *et al.* (2004); [9] St-Onge *et al.* (2003).

2.2 Core processing and continuous logging

In the laboratory, the wet bulk density and low field volumetric whole core magnetic susceptibility (k) of cores 12PC, 28PC and 27bLEH were determined using a GEOTEK Multi Sensor Core Logger (MSCL) at ISMER. The cores were also ran through a CAT-scan (computerized axial tomography) at INRS-ETE for the identification of sedimentary structures and extraction of CT-number profiles (see St-Onge *et al.* 2007 for details) and then split, photographed and described. CT number profiles primarily reflect changes in bulk density (St-Onge *et al.* 2007; see also Figs. 3-5). Similarly, lacustrine cores from Chilean Andes and the French Alps were measured using a GEOTEK MSCL at the GZF Potsdam and at the ETH Zurich, respectively (cf. Chapron *et al.* 2005; Chapron *et al.*, 2007).

Micro-fluorescence-X (XRF) analyses were performed with an ITRAX core scanner (see Croudace *et al.* 2006 or St-Onge *et al.* 2007 for details) on core BRA03-1 with a downcore resolution of 300 µm and an irradiation time of 1 s. The radiographs obtained were transformed in negative X-ray images. Color reflectance measurements were performed on cores 28PC and 27bLEH using a hand-held X-rite DTP22 digital swatchbook spectrophotometer. Reflectance data are reported as a* from the widely used International Commission on Illumination (CIE) color space, whereas a* ranges from +60 (red) to -60 (green). Variations in a* values are often associated with changes in the concentration of red minerals, such as hematite and were, for example, used by Hall *et al.* (2001) to identify a red bed layer in Hudson Strait sediments.

Low-field volumetric magnetic susceptibility (k) was also measured on u-channel samples (rigid u-shaped plastic

liners with a square 2-cm cross-section and a length of 1.5 m) using the recently installed magnetic susceptibility track at the University of Florida (Thomas *et al.* 2003) at 1 cm intervals on cores 750 and 124. Low-field volumetric magnetic susceptibility primarily reflects changes in the concentration of ferrimagnetic minerals such as magnetite, but is also influenced by large magnetite grains (*e.g.*, Stoner *et al.* 1996; Stoner and St-Onge 2007). In addition, an anhysteretic remanent magnetization (ARM) was produced using a 100 mT peak alternating field and a 50 μT direct current biasing field and subsequently measured at the University of Florida using a 2G Enterprises Model 755 cryogenic magnetometer at 1 cm intervals. ARM is primarily responding to changes in the concentration of ferrimagnetic minerals, but is also strongly grain size dependant, being particularly influenced by magnetite grain sizes <10 μm (*e.g.*, Stoner *et al.* 1996; Stoner and St-Onge 2007).

2.3 Grain size analyses

For core LDB11a, grain size analyses were performed at high resolution (every 0.5 cm) without any pre-treatment using the Malvern Mastersizer X laser sizer from Savoie University (France). For all the other cores presented in this paper, grain size analyses were carried out at ISMER with a sampling interval ranging from 10 to 0.5 cm depending on the facies and core characteristics. Disaggregated samples were analyzed with a Beckman-Coulter LS-13320 (0.04 to 2000 μm) laser sizer. The results of at least three runs were averaged. The average continuous disaggregated particle size distribution output was then processed using the Gradistat software for sediment parameters (Blott and Pye 2001).

2.4 Anisotropy of the magnetic susceptibility (AMS)

In core LDB11a, a continuous sampling of 2 cm^3 plastic cubes and their measurement using a Kappabridge KLY-2 magnetometer at Lille University (France) allowed documenting the anisotropy of the magnetic susceptibility (AMS) of these lacustrine sediments. The AMS of a sample can be represented geometrically by an ellipsoid characterized by the three orthogonal axes defined as the maximum, intermediate and minimum susceptibilities (K_1, K_2, and K_3, respectively; Fig. 2). Two parameters derived from these susceptibilities are often used to characterize the form of the ellipsoid: the magnetic lineation ($L=K_1/K_2$) and foliation ($F=K_2/K_3$). These two parameters respectively reflect the linear or planar magnetic fabric.

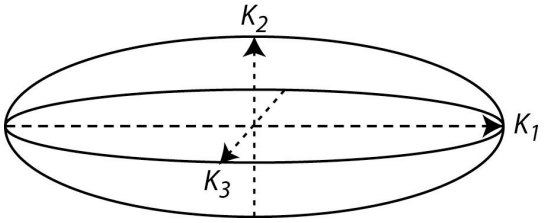

Figure 2. Illustration of the three orthogonal axes of the magnetic susceptibility ellipsoid.

3. RESULTS

3.1 Identification and characterization of rapidly deposited layers (RDL)

In this section, we will overview five case studies from different parts of the world (Eastern Canada, Hudson Bay and Strait, the Alps and Patagonia) and different environments (ocean and lake) where the continuous physical and magnetic properties of the sediment where used in conjunction with traditional sedimentological analyses to identity and characterize rapidly deposited layers (RDL).

3.1.1. Example from the Gulf of St. Lawrence (Eastern Canada)

In this first example from the Gulf of St. Lawrence (Fig. 1 and Table 1), a RDL with a minimum thickness of 57 cm is observed in core 12PC from 343 to 286 cm (Fig. 3). The CAT-scan image reveals parallel and sub-horizontal laminations at the base of the RDL, whereas the density, CT number and magnetic susceptibility profiles indicate a coarse base and a normal grading. This grading is confirmed by the grain size analyses and indicates the deposition of a classical normal graded turbidite (Bouma 1962).

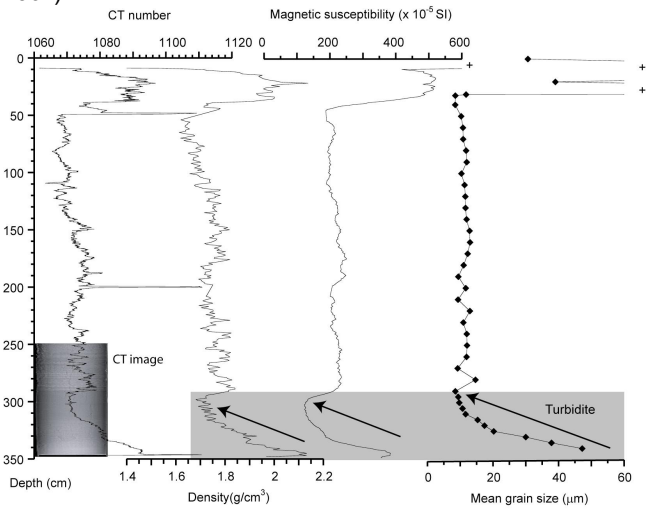

Figure 3. Physical, magnetic and sedimentological properties of core 12PC (Gulf of St. Lawrence). The grey area highlights the presence of a normal graded turbidite. From Lajeunesse *et al.* (2007)

3.1.2. Example from Hudson Bay and Strait

In this second example from Hudson Bay and Strait (Fig. 1 and Table 1), while both cores are from different areas and thus different overall sedimentological regime, the a* profiles clearly allow the identification of a distinctive red bed from about 150 cm to the base of core 27bLEH (Fig. 4) and from 296 to 304 cm in core 28PC (Fig. 5). In core 27bLEH, magnetic susceptibility values are relatively high and mirror changes in density and grain size, indicating that they are mostly reflecting changes in magnetic grain size, whereas in core 28PC, the reddish interval is characterized by lower

magnetic susceptibility, density and CT number values. Grain size values within these two intervals are also different from the rest of the core, with lower mean grain size in core 28PC and higher sand contents in core 27bLEH. In addition, the sand percent, magnetic susceptibility, density and CT number profiles also highlight two clear sequences of reverse and normal grading in core 27bLEH (Fig. 4), suggesting the deposition of two hyperpycnal deposits (Mulder *et al.* 2001; 2003; St Onge *et al.* 2004; Schneider *et al.* 2004; Chapron *et al.* 2006; St-Onge and Lajeunesse 2007). St-Onge and Lajeunesse (2007) interpreted this sequence as the result of a two-pulse flood of the final drainage of Lake Agassiz-Ojibway.

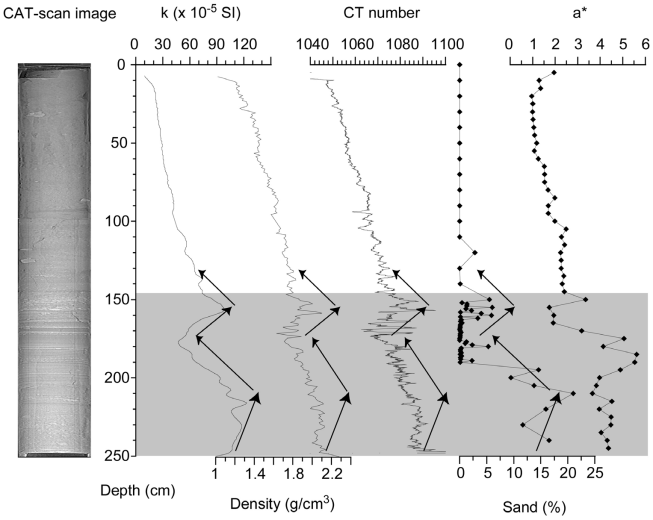

Figure 4. Magnetic, physical and grain size analyses of core 27bLEH. The grey zone highlights the reddish layer. From St-Onge and Lajeunesse (2007).

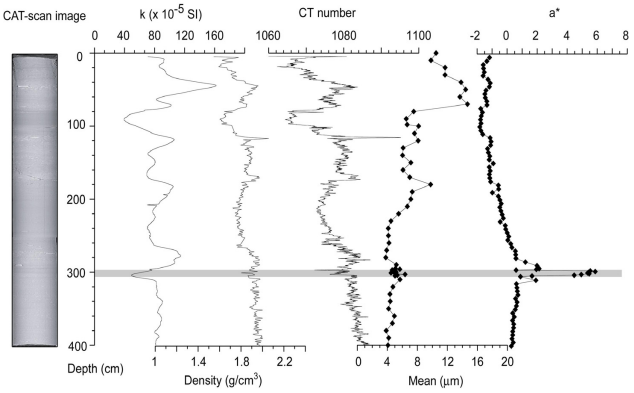

Figure 5. Magnetic, physical and grain size analyses of core 28PC. The grey zone highlights the reddish layer. From St-Onge and Lajeunesse (2007).

3.1.3. Example from Lake Bramant (French Alps)

In this third example from Alpine lacustrine sediments (Lake Bramant, Fig. 1 and Table 1), the combination of physical and sedimentological data allowed the identification of two relatively thin RDLs, labelled E2 and E3, at 25-28 cm and 31-35 cm, respectively (Fig 6, see also Fig. 10). In the 4 cm-thick sedimentary event E3 (Fig. 6b), the basal sequence is characterized by an inverse grading (coarsening upward). The middle of the deposit (around 33 cm) is characterized by a thin layer of very fine sand, notably highlighted by a lighter grey scale and by a peak in the CT number, indicating a higher bulk density. Above the sand layer, the different proxies are reflecting a normal grading (fining upward). This grain size evolution is typical of hyperpycnal flows generated by large flood events in marine or lacustrine environments (e.g., Mulder *et al.* 2001; 2003; St-Onge *et al.* 2004; Schneider *et al.* 2004; Chapron *et al.* 2006; St-Onge and Lajeunesse 2007). The waxing flow (rising limb of the flood) results in the development of the inversely graded bed up to the peak of the flood, whereas the waning flow (falling limb of the flood) results in the subsequent normal grading. The distribution of very fine sands and evolution of mean grain size in the 4 cm-thick sedimentary event E2 (Fig. 6a) depict the development of a normally-graded sequence starting with a coarse base sharply fining upward. E2 is interpreted as a large flood-induced turbidite either related to the formation of a hyperpycnal flow, where only the upper sequence was preserved because of strong erosion during the rising limb of the flood (Mulder *et al.* 2001; Mulder *et al.* 2003), or to the development of a large homopycnal flow across the lake (Brodzikowski and Van Loon 1991). The formation of such exceptional flood deposits in Lake Bramant may result from the catastrophic drainage (i.e., outburst) of a temporary ice-contact lake or even a subglacial lake.

Grain size trends in RDLs E2 and E3 are also highlighted by Fe/Rb and Rb fluctuations. A Fe enrichment was previously interpreted as an indicator of the coarse base of turbidites, whereas variations of the Rb content were related to fluctuations in the amount of detrital clays (Rothwell *et al.* 2006). Similarly, Fe in Lake Bramant sediments is concentrated in the coarse fraction especially at the base of turbidites (higher Fe/Rb ratio), whereas the Rb content reflects the finer sediment fluctuations associated with the “glacial flour” resulting from glacial erosion.

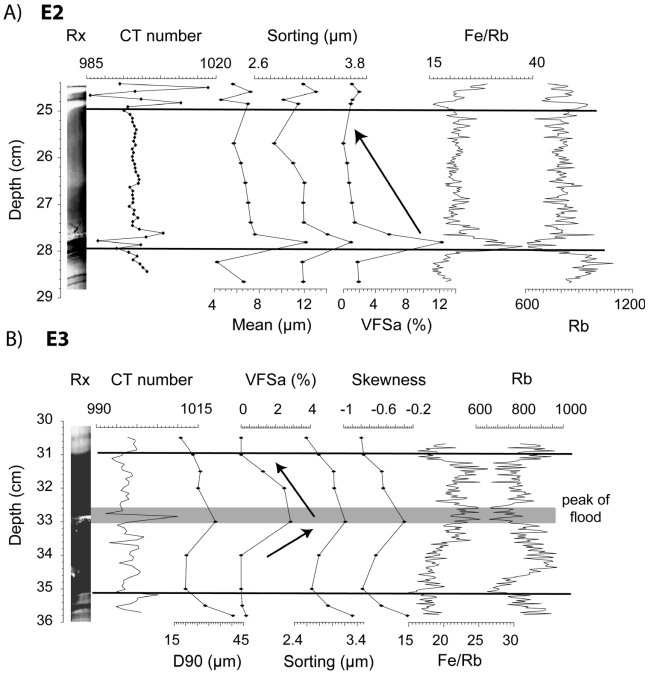

Figure 6. Sedimentary events E2 (A) and E3 (B) from core BRA03-1 (Lake Bramant). Rx images are obtained from the ITRAX measurements; VFSa: very fine sand percent (from 63 to 125 µm). Modified from Guyard *et al.* (2007b).

3.1.4. Example from Lake Le Bourget (French Alps)

In the deepest part of Lake Le Bourget (French Alps, Fig. 1 and Table 1), a very homogenous RDL was previously identified by Chapron *et al.* (1999) and associated with the strong (VII-VIII MSK intensity) historical AD 1822 earthquake. During this earthquake, several coeval subaqueous slides and a violent lake water oscillation (i.e., a seiche effect) were reported and triggered the deposition of a seiche deposit (labelled H in Fig. 7). This deposit is characterized by a coarse base and a thick homogenous silty clay upper unit as shown by the grain size evolution.

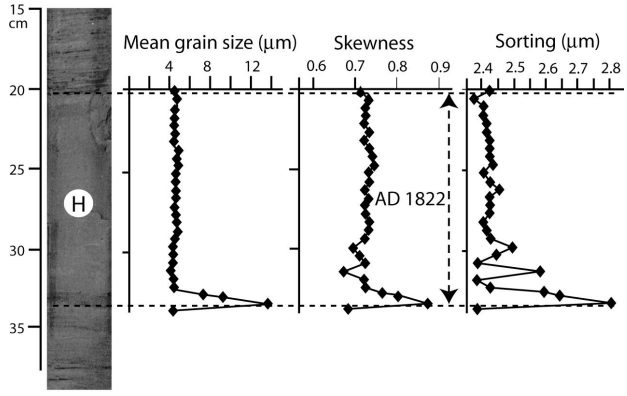

Figure 7. Core photograph and high resolution grain size analyses in the AD 1822 seiche deposit of core LDB11a from Lake Le Bourget (modified from Chapron *et al.* 1999).

In addition, the first centimetres of this seiche deposit (H) are highlighting significant fluctuations in the skewness and sorting parameters (Fig. 7), but a clear peak in magnetic foliation (Fig. 8). This signature is clearly contrasting with the upper part of the seiche deposit characterized by a homogenous mean grain size, stable skewness and sorting parameters and a clear peak in magnetic foliation and lineation (Figures 7 and 8). Below this seiche deposit, three sharp based dark grey clayey layers are also highlighted by higher values in mean magnetic susceptibility and in magnetic foliation (Fig. 8). The most recent of these dark grey layers is additionally bearing a clear peak in magnetic lineation.

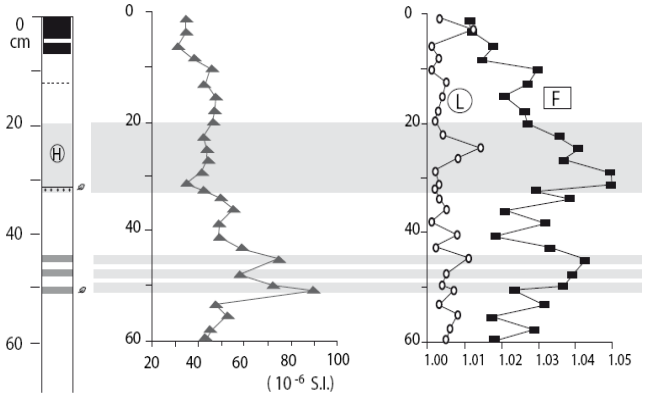

Figure 8. Synthetic lithology and magnetic properties of core LDB 11a from Lake Le Bourget (modified from Chapron 1999): mean magnetic susceptibility (grey triangles); magnetic lineation (white circles, L); magnetic foliation (black rectangles, F). Legend: black=biochemical varves, white=faintly laminated marls, light grey=the AD 1822 seiche deposit, dark grey=clayey flood deposits.

These three lower RDL are rich in minerogenic materials (producing high mean magnetic susceptibility values) previously identified on several short cores and are related to catastrophic Rhone River flood events induced during the Little Ice Age (LIA) by increasing glacier activity in the Mont Blanc Massif and by the down stream propagation of a braided pattern in the Rhone River (Chapron *et al.* 2005). The planar sedimentary fabric of these flood deposits in the deep basin of Lake Le Bourget deduced from their high values of magnetic foliation indicates here that these layers result from the final settling of fine grained sediment plumes produced by hyperpycnal flood events. An additional peak in magnetic lineation in the upper flood deposit (Fig. 8) is here interpreted as reflecting the settling of a fine grained sediment plume under a rather weak current developed along the lake floor.

3.1.5. Example from Lake Puyehue (Chilean Patagonia)

In this last example from lacustrine environment, X-ray radiography at the base of core PU-I-P4 was used to disentangle background sedimentation from intercalated RDLs related to historical volcanic eruptions and to the impact of the nearby AD 1960 Valdivia subduction earthquake (Mw 9.5). In Fig. 9, the AD 1907 tephra layer and the AD 1960 earthquake-induced pumices are clearly identified. As detailed in Chapron *et al.* (2007), these

pumices were reworked from the catchment area after the Puyehue volcano eruption and constitute the base of a mega flood event starting with an erosive surface and developing thick laminations denser than in background sediments (Fig. 9).

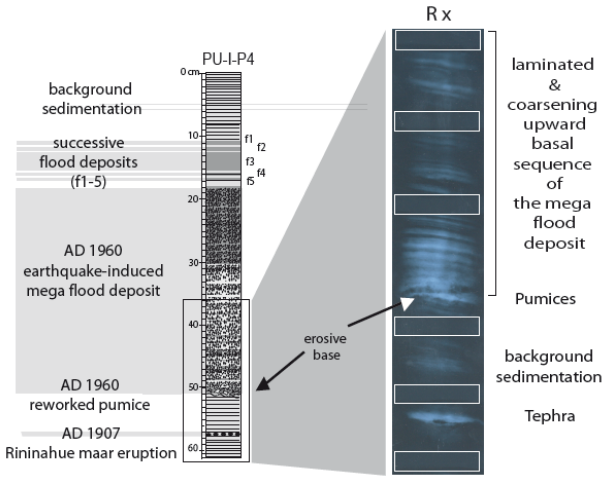

Figure 9. Lithology of core PU-I-P4 and X-rays illustrating the contrasting facies of background sedimentation (biogenic varves), volcanic deposits (pumices and tephra layers) and the laminated basal sequence of the AD 1960 earthquake-induced flood deposit. White rectangles on the X-rays correspond to sections sampled for radiometric measurements. Modified from Chapron *et al.* (2007).

3.2 Correlation and dating of rapidly deposited layers

In this section, we will present six case studies where the continuous physical and magnetic properties of the sediments were used to date rapidly deposited layers. The dating was performed either directly by allowing the counting of varves or by correlation to previously dated cores or layers.

3.2.1. Example from Lake Bramant

In the study discussed above (section 3.1.3.) on the identification of two RDLs from Lake Bramant (French Alps, Fig. 1 and Table 1), Guyard *et al.* (2007a) used the combination of a digital X-ray image derived from the ITRAX core scanner and the CT number profile derived from the CAT-scan image to identify and count varves (Fig. 10) to derive an age model. The varve count was confirmed by ^{137}Cs and ^{241}Am measurements and indicates that RDL E2 and E3 were respectively deposited in 1908 and 1904. Similarly, in the lower part of the record (not shown), the varves were counted using the Fe content and confirmed by AMS ^{14}C dates (Guyard *et al.* 2007a). According to the ages derived from the varve count and to the first field observations in AD 1907 (Fuselin *et al.* 1909), the exceptional flood events E2 and E3 thus occurred when the St. Sorlin glacier was already retreating from its last advance following the end of the Little Ice Age (LIA). Exceptional flood events in Lake Bramant could thus be linked to climatic oscillations through the outbursts of temporary ice contact lakes or subglacial lakes during warmer periods.

3.2.2. Example from Lake Le Bourget (NW Alps)

In the deep basin of Lake Le Bourget, the chronology of core LDB11a is based on correlation of key sedimentary events (i.e. the initiation of biochemical varve formation, the seiche deposit and basin wide catastrophic flood deposits) that are dated by radionuclide (^{210}Pb and ^{137}Cs) and by the correlation of RDL with historical events when applying a mean sedimentation rate to the background sedimentation (i.e. faintly laminated marls dated by radionuclide and by radiocarbon; cf. Chapron *et al.*, 2002; 2005). This age-depth model allows correlating the seiche deposit with the AD 1822 Chautagne earthquake and a large flood deposit (the second one) with the oldest historical flood event of the Rhone River in AD 1732 (cf. Chapron *et al.* 2002).

3.2.3. Example from Lake Puyehue (Chilean Andes)

In the deep basin of Lake Puyehue facing the Golgol River delta, the chronology of core PU-I-P4 is based on a combination of radionuclide dating (^{210}Pb and ^{137}Cs) and on tephrostratigraphy, allowing the correlation of a coarse tephra layer with the AD 1907 Rininahue maar eruption in the Puyehue volcanic complex (cf. Chapron *et al.*, 2007). In addition, the combination of high-resolution seismic reflection data, field work in the catchment area of the Golgol River together with historical chronicles allowed Chapron *et al.* (2007) to link the hyperpycnal deposit (flood deposit of Fig. 9) with the outburst of several earthquake-induced landslide dams across the Golgol River, a couple of weeks after the end of the AD 1960 Puyehue earthquake-induced volcanic eruption.

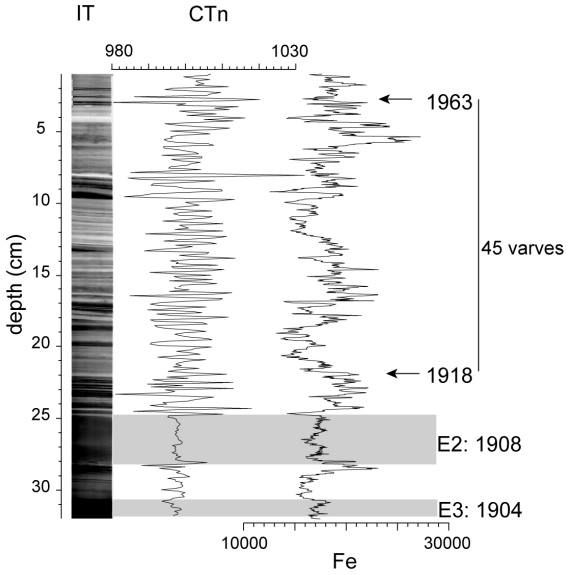

Figure 10. Details of the age-depth model in the upper part of core BRA03-1. The varves were counted by "CT number peak counting". IT: Rx obtained by ITRAX core scanner analysis; CTn: CT number. Modified from Guyard *et al.* (2007a).

3.2.4. Example from Hudson Bay and Strait

A reddish layer similar to the one discussed above (section 3.1.2.) and associated with the final drainage of Lake Agassiz-Ojibway (Barber *et al.* 1999) was previously identified in Hudson Strait sediments and used as a regional stratigraphic isochron (Kerwin 1996). In a core (core 101; Fig. 1 and Table 1) recovered from a site located nearby core 28PC, the red bed contrasted sharply from the rest of the core with relatively lower magnetic susceptibility values and higher a* values (Kerwin 1996; Hall *et al.* 2001). Based on the magnetic susceptibility profiles of cores 28PC and 101, we can easily correlate them (Fig. 11). Based on that correlation and by correcting the ^{14}C ages presented by Kerwin (1996) using new radiocarbon reservoir age data (McNeely *et al.*, 2006), the age of the red bed can be estimated between 7760 and 7860 yr BP (conventional ^{14}C date corrected by -590 yrs; Lajeunesse and St-Onge in press), which is close to the estimated date of 7700 yr BP (8470 cal yr BP) for the final drainage of Lake Agassiz-Ojibway (Barber *et al.* 1999). Finally, because the same series of events is observed in the reddish layer of cores 28PC and 27bLEH, St-Onge and Lajeunesse (2007) suggested that the red bed was synchronous and that the coarser grain size and the pronounced thickness of core 27bLEH reddish layer indicate a more proximal sediment source.

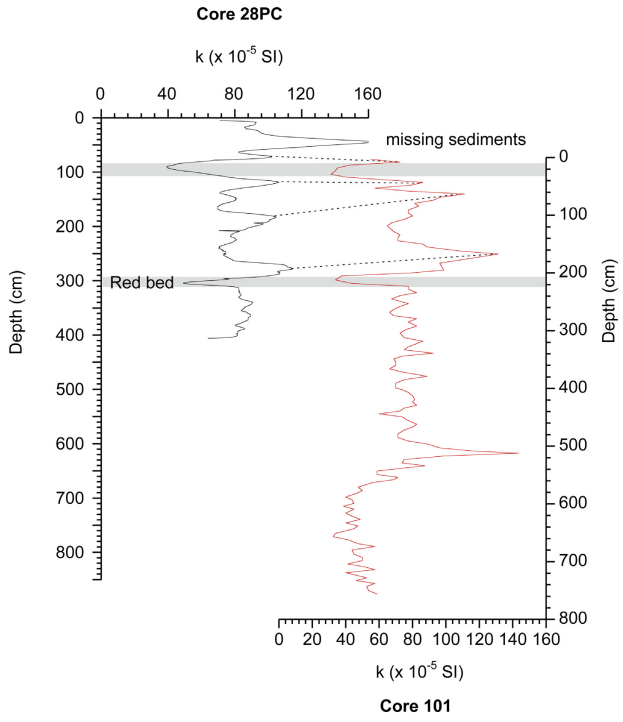

Figure 11. Correlation of core 28PC to core 101 (Kerwin 1996) from Hudson Strait. Two low magnetic susceptibility horizons of similar values, including the reddish layer, are highlighted and used for correlation. Several other magnetic susceptibility highs can be correlated and are illustrated by dashed lines. From St-Onge and Lajeunesse (2007).

3.2.5. Example from the Beaufort Sea and Amundsen Gulf

In a recent study, Scott *et al.* (subm.) identified a specific interval of ice rafted debris (IRD) in a core (124) from the Amundsen Gulf, Western Canadian Arctic (Fig. 1 and Table 1). This interval is characterized by coarser and poorly sorted sediments reflected notably by higher magnetic susceptibility and grain size values, as well as by higher sorting values (not shown). A two-peak structure in the magnetic properties (k) is observed, while two radiocarbon dates obtained in that IRD interval suggest an age of about 11.5 kyr BP (Fig. 12a).

Based on the magnetic measurements, the IRD interval observed in core 124 can be correlated with the upper part of core 750 (Fig. 1 and Table 1). Indeed, the upper part of the magnetic susceptibility and ARM profiles of both cores can easily be correlated, with the two-peak structure observed in core 124 also found in core 750 (Fig. 12 a-b). Below these two coincident peaks, the correlation is unclear and likely reflects the very different nature of both sediment cores below the IRD interval. Below that zone, core 124 is much richer in organic matter with root fragments and some sand (Scott *et al.* subm.). This is not the case for core 750.

3.2.6. Example from the Saguenay Fjord

In this example, St-Onge *et al.* (2004) recovered a 38 m-long piston core (2222) from the deep basin of the Saguenay Fjord, Québec (Fig 1 and Table 1) and, using high-resolution physical, magnetic and sedimentological analyses, identified at least 14 RDLs that they interpreted to be either directly or indirectly associated with major earthquakes. In this case study, dating the RDLs was difficult notably because $CaCO_3$ dissolution occurs in the sediments of the Saguenay Fjord (St-Onge *et al.* 1999). Nevertheless, one benthic mollusk shell was found in "background" hemipelagic sediments and dated. The interval of hemipelagic sediment between this date and the base of the uppermost RDL accumulated at a rate of 0.15 cm/yr. This estimate is consistent with a sedimentation rate of 0.18 cm/yr determined using ^{210}Pb measurements in the top of core 2222 and with rates calculated using ^{137}Cs and ^{210}Pb measurements in box-cored sediments from surrounding sites (e.g., Smith and Walton 1980; St-Onge and Hillaire-Marcel 2001). Using the 0.15 cm/yr sedimentation rate, the full magnetic vector of core 2222 "background" sediments was then correlated with the Holocene paleomagnetic record of core 2220, raised from the St. Lawrence Estuary (Fig.1 and Table 1; St-Onge *et al.* 2003). This exercise resulted in a good correlation to core MD99-2220 inclination, declination and relative paleointensity proxy (Fig. 13) records. Core MD99-2220 chronology is primarily based on thirteen ^{14}C AMS dates and is in good agreement with the Greenland Ice Sheet Project (GISP2) chronology and the tree-ring chronology of Stuiver *et al.* (1998) for the last ~8500 cal BP (St-Onge *et al.* 2003). The resulting chronology revealed that the base of core MD99-2222 is about 7200 cal BP.

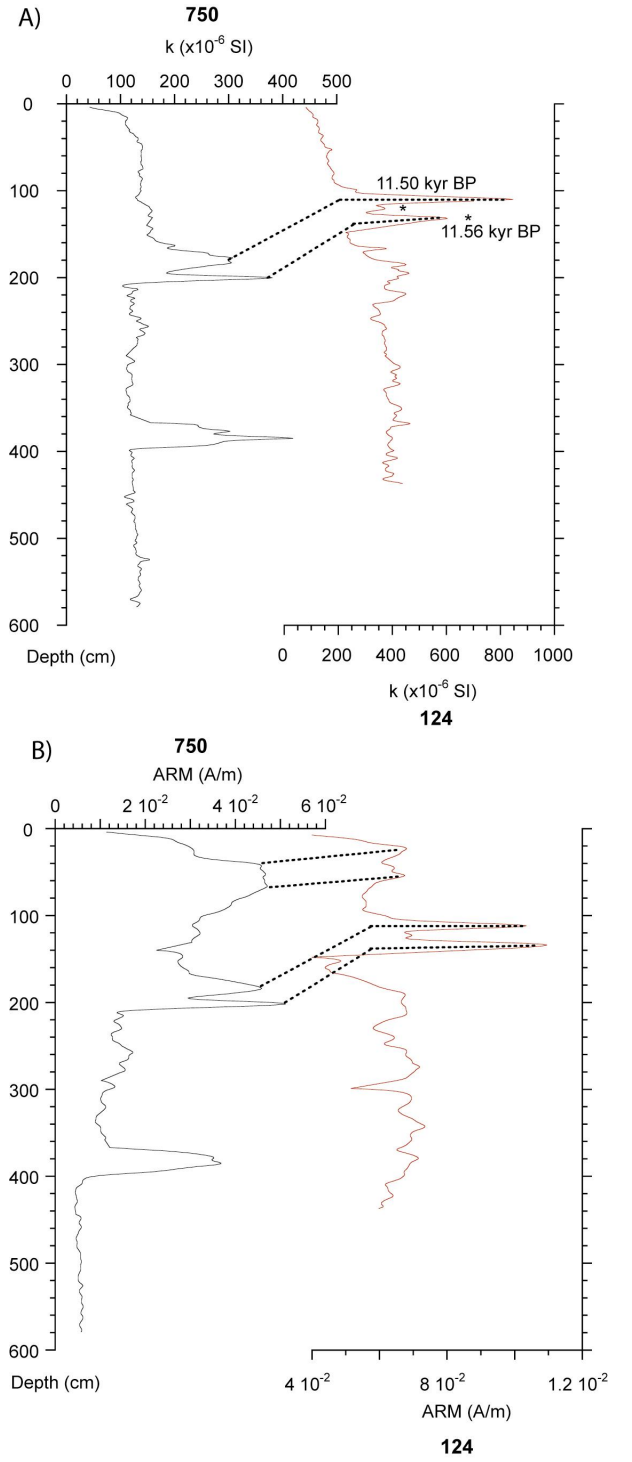

Figure 12. Comparison of A) low field volumetric magnetic susceptibility (k) and B) anhysteretic remanent magnetization (ARM) of cores 750 and 124. Dashed lines indicate correlative features. ^{14}C dates obtained on mixed foraminifera are also illustrated. The dates are reported in radiocarbon years and are uncorrected for reservoir effects. Modified from Scott *et al.* (subm.).

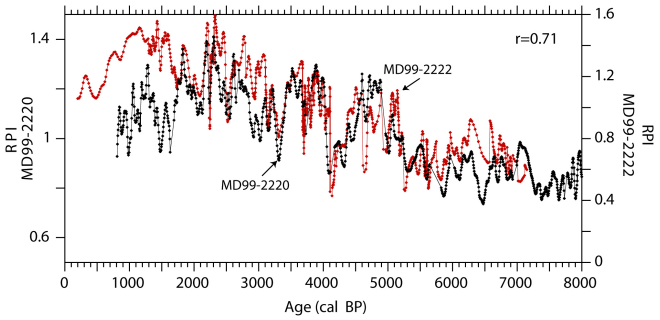

Figure 13. Comparison of core 2222 (Saguenay Fjord) and 2220 (St. Lawrence Estuary) relative paleointensity (RPI) records.

4. CONCLUSIONS

In this paper, we have shown that the combination of continuous physical and magnetic properties with traditional sedimentological analyses can be a powerful tool to identify, characterize and date rapidly deposited layers in different sedimentary environments. The analyses can be used to help determine the trigger mechanism of the rapidly deposited layers and to date these layers either directly or indirectly. Furthermore, these methods have the advantage of being rapid, continuous and non destructive.

5. ACKNOWLEDGMENTS

The authors wish to thank the various captains, crew and colleagues who contributed to the collection of the sediment cores presented in this overview paper. These studies were supported by NSERC through Discovery and ship time grants, the Canadian Arctic Shelf Exchange Program, ArcticNet and le *Fonds québécois de la recherche sur la nature et les technologies*, while studies in France were supported by the ECLIPSE program (CNRS-INSU) and by the French Mountain Institute (Savoie University). We also thank J.T. Andrews (INSTAAR) for generously sharing core 101 magnetic susceptibility data, and Flavio Anselmetti (Eawag) and Roger Urgeles (*Universitat de Barcelona*) for their constructive reviews. Finally, we thank Karine Tessier (Laval University) for drawing Figure 1. This is GEOTOP Publication n° 2008-0013.

6. REFERENCES

Barber, D.C., Dyke, A., Hillaire-Marcel, C., Jennings, A.E., Andrews, J.T., *et al.*, 1999. Forcing of the cold event of 8,200 years ago by catastrophic drainage of Laurentide lakes. *Nature*, Vol. 400, pp. 344–348.

Blott, S.J., and Pye, K., 2001. Gradistat: a grain size distribution and statistics package for the analysis of unconsolided sediments. *Earth Surf. Process. Landforms*, Vol. 26, pp. 1237-1248.

Bouma, 1962. Sedimentology of Some Flysch Deposits. A graphic approach to facies interpretation. Elsevier, Amsterdam, 168 p.

Brodzikowski, K., and Van Loon, A.J., 1991. Review of glacigenic sediments. *Development in Sedimentology*, Vol. 49, 688 p.

Chapron, E., Juvigné, E., Mulsow, S., Ariztegui, D., Magand, O., Bertrand, S., Pino, M., and Chapron, O., 2007. Clastic sedimentation processes in Lago Puyehue: Implications for natural hazards and paleoenvironment reconstructions in the Chilean Lake District, 40.5°S. *Sedimentary Geology*, Vol. 201, pp. 365-385.

Chapron, E., Ariztegui, D., Mulsow, S., Villarosa, G., Pino, M., *et al.*, 2006. Impact of the 1960 major subduction earthquake in Northern Patagonia. *Quaternary International*, Vol. 158, pp. 58-71 .

Chapron, E., Arnaud, F., Noël, H., Revel, M., Desmet, M., and Perdereau, L., 2005. Rhone River flood deposits in Lake Le Bourget: a proxy for Holocene environmental changes in the NW Alps, France. *Boreas*, Vol. 34, pp.1-13.

Chapron, E., Desmet, M., De Putter T., Loutre, M. F., Beck, C., and Deconinck, J.F., 2002. Climatic variability in the northwestern Alps, France, as evidenced by 600 years of terrigenous sedimentation in Lake Le Bourget. *The Holocene*, Vol. 12, pp. 177-185.

Chapron, E., Beck, C., Pourchet, M., and Deconinck, J-F., 1999. 1822 earthquake-triggered homogenite in Lake Le Bourget (NW Alps). *Terra Nova*, Vol. 11, pp. 86-92.

Chapron, E., 1999. Contrôles climatique et sismo-tectonique de la sédimentation lacustre dans l'Avant-pays alpin (Lac du Bourget, Léman) durant le Quaternaire récent. *Géologie Alpine*, mem. hs. N° 30, 258 p.

Croudace, I.W., Rindby, A., and Rothwell, R.G., 2006. ITRAX: description and evaluation of a new X-Ray core scanner. In: R.G. Rothwell (Ed.), New Techniques in Sediment Core Analysis. *Geol. Soc. Spec. Publ*. Vol. 267, pp. 51-63.

Fuselin, G., Jacob, C., and Offner, J., 1909. Études glaciaires, géographiques et botaniques dans le massif des Grandes Rousses. Études glaciologiques, Ministère de l'Agriculture, Paris, pp. 107-112.

Guyard, H., Chapron, E., St-Onge, G., Anselmetti, F., Arnaud, F., Magand, O., Francus, P., and Mélières, M.-A., 2007a. High-altitude varve records of abrupt environmental changes and mining activity over the last 4000 years in the Western French Alps (Lake Bramant, Grandes Rousses Massif). *Quaternary Science Reviews*, Vol. 26, pp. 2644-2660.

Guyard, H., St-Onge, G., Chapron, E., Anselmetti, F., and Francus, P., 2007b. The AD 1881 earthquake-triggered slump and late Holocene exceptional flood-induced turbidites from proglacial Lake Bramant, Western French Alps. In: V. Lykousis, D. Sakellariou and J. Locat (Eds.), Submarine Mass Movements and Their Consequences. Springer, pp. 279-286.

Hall, F.R., Andrews, J.T., Kerwin, M., and Smith, L.M., 2001. Studies of sediment colour, whole-core magnetic susceptibility, and sediment magnetism of Hudson Strait-Labrador Shelf region: CSS Hudson cruises 90023 and 93034. In: B. MacLean (Ed.), Late Quaternary sediments, depositional environments, and Late Glacial/Deglacial history derived from marine and terrestrial studies. *Geol. Survey of Canada Bulletin*, Vol. 566, pp. 161-170.

Kerwin, M.W., 1996. A regional stratigraphic isochron (ca. 8000 ^{14}C yr B.P.) from final deglaciation of Hudson Strait. *Quaternary Research*, Vol. 46, pp. 89-98.

Lajeunesse, P., and St-Onge, G., in press. Subglacial origin of Lake Agassiz-Ojibway final outburst flood. *Nature Geoscience*.

Lajeunesse, P., St-Onge, G., Labbé, G., and Locat, J., 2007. Morphosedimentology of submarine mass-movements and gravity flows offshore Sept-Îles, NW Gulf of St. Lawrence (Québec, Canada). In: V. Lykousis, D. Sakellariou and J. Locat (Eds.), Submarine Mass Movements and Their Consequences. Springer, pp. 129-137.

McNeely, R., Dyke, A.S., and Southon, J.R. 2006. Canadian marine reservoir ages, preliminary data assessment, *Geological Survey of Canada, Open File 5049*.

Mulder, T., Syvitski, J. P. M., Migeon, S., Faugères, J-C., and Savoye, B., 2003. Marine hyperpycnal flows : initiation, behavior and related deposits. A review. *Marine and Petroleum Geology*, Vol. 20, pp. 861-882.

Mulder, T., Migeon, S., Savoye, B., and Jouanneau, J.-M., 2001. Twentieth century floods recorded in deep Mediterranean sediments. *Geology*, Vol. 29, pp. 1011-1014.

Rothwell, R. G., Hoogakker, B., Thomson, J., Croudace, I. W., and Frenz, M., 2006. Turbidite emplacement on the southern Balearic Abyssal Plain (western Mediterranean Sea) during Marine Isotope Stages 1-3: an application of ITRAX XRF scanning of sediment cores to lithostratigraphic analysis. In: R.G. Rothwell (Ed.), New Techniques in Sediment Core Analysis. *Geol. Soc. Spec. Publ*. Vol. 267, pp. 79-98.

Schneider, J-L., Pollet, N., Chapron, E., Wessels, M., and Wassmer, P., 2004. Signature of Rhine Valley sturzstrom dam failures in Holocene sediments of Lake Constance, Germany. *Sedimentary Geology,* Vol. 169, pp. 75-91.

Scott, D.B., Schell, T., St-Onge, G., Rochon, A., and Blasco, S. submitted. Foraminiferal assemblage changes over the last 15,000 years on the McKenzie/Beaufort Sea slope and Amundsen Gulf, Canada: implication for past sea-ice conditions. *Paleoceanography*.

Smith, J.N., and Walton, A., 1980. Sediment accumulation rates and geochronologies measured in the Saguenay Fjord using Pb-210 dating method. *Geochimica et Cosmochimica Acta*, Vol. 44, pp. 225-240.

Stoner, J.S., Channell, J.E.T., and Hillaire-Marcel, C. (1996), The magnetic signature of rapidly deposited detrital layers from the deep Labrador sea: relationship to North Atlantic Heinrich layers. *Paleoceanography*, Vol. 11, pp. 309-325.

Stoner, J.S., and St-Onge, G. 2007. Magnetic stratigraphy in paleoceanography: reversals, excursions, paleointensity and secular variation. In: C. Hillaire-Marcel and A. de Vernal (Eds.), Proxies in Late Cenozoic Paleoceanography, Elsevier, pp. 99-137.

St-Onge, G., and Lajeunesse, P. 2007. Flood-induced turbibites from northern Hudson Bay and western Hudson Strait: a two-pulse record of Lake Agassiz final outburst flood? In: V. Lykousis, D. Sakellariou and J. Locat (Eds.), Submarine Mass Movements and Their Consequences. Springer, pp. 129-137.

St-Onge, G., Mulder, T., Francus, P., and Long., B. 2007. Continuous physical properties of cored marine sediments. In: C. Hillaire-Marcel and A. de Vernal (Eds.),

Proxies in Late Cenozoic Paleoceanography, Elsevier, pp. 63-98.

St-Onge, G., Mulder, T., Piper, D.J.W., Hillaire-Marcel, C., and Stoner, J.S., 2004. Earthquake and flood-induced turbidites in the Saguenay Fjord (Québec): a Holocene paleoseismicity record. *Quaternary Science Reviews*, Vol. 23, pp. 283-294.

St-Onge, G., Stoner, J.S., and Hillaire-Marcel, C., 2003. Holocene paleomagnetic records from the St. Lawrence Estuary: centennial- to millennial-scale geomagnetic modulation of cosmogenic isotopes. *Earth and Planetary Science Letters*, Vol. 209, pp. 113-130.

St-Onge, G., and Hillaire-Marcel, C., 2001. Isotopic constraints of sedimentary inputs and organic carbon burial rates in the Saguenay Fjord, Quebec. *Marine Geology*, Vol. 176, pp. 1-22.

St-Onge, G., Leduc, J., Bilodeau, G., de Vernal, A., Devillers, R., *et al.*, 1999. Caractérisation des sédiments récents du fjord du Saguenay à partir de traceurs physiques, géochimiques, isotopiques et micropaléontologiques. *Géographie physique et Quaternaire*, Vol. 53, pp. 339-350.

Stuiver, M., Reimer, P.J., Bard, E., Beck, J. W., Burr, G.S., *et al.*, 1998. INTCAL98 radiocarbon age calibration, 24,000-0 cal BP. *Radiocarbon*, Vol. 40, pp. 1041-1083.

Thomas, R.G., Guyodo, Y., and Channell, J.E.T. (2003), U channel track for susceptibility measurements. *Geochemistry, Geophysics, Geosystems*, Vol. 4, 1050, doi:10.1029/2002GC000454.